PRL 94, 232002 (2005) PHYSICAL REVIEW LETTERS week ending 17 JUNE 2005

Branching Fractions for $\psi(2S)$-to-J/ψ Transitions

(CLEO Collaboration)

Abstract

We describe new measurements of the inclusive and exclusive branching fractions for $\psi(2S)$ transitions to J/ψ using e^+e^- collision data collected with the CLEO detector operating at CESR. All branching fractions and ratios of branching fractions reported here represent either the most precise measurements to date or the first direct measurements. Indirectly and in combination with other CLEO measurements, we determine $\mathcal{B}(\chi_{cJ} \to \gamma J/\psi)$ and $\mathcal{B}[\psi(2S) \to$ light hadrons$]$.

Introduction

branching fraction measurements of 4 exclusive hadronic transitions

$\psi(2S) \to J/\psi + h$

$(h = \pi^+\pi^-, \pi^0\pi^0, \eta, \pi^0)$

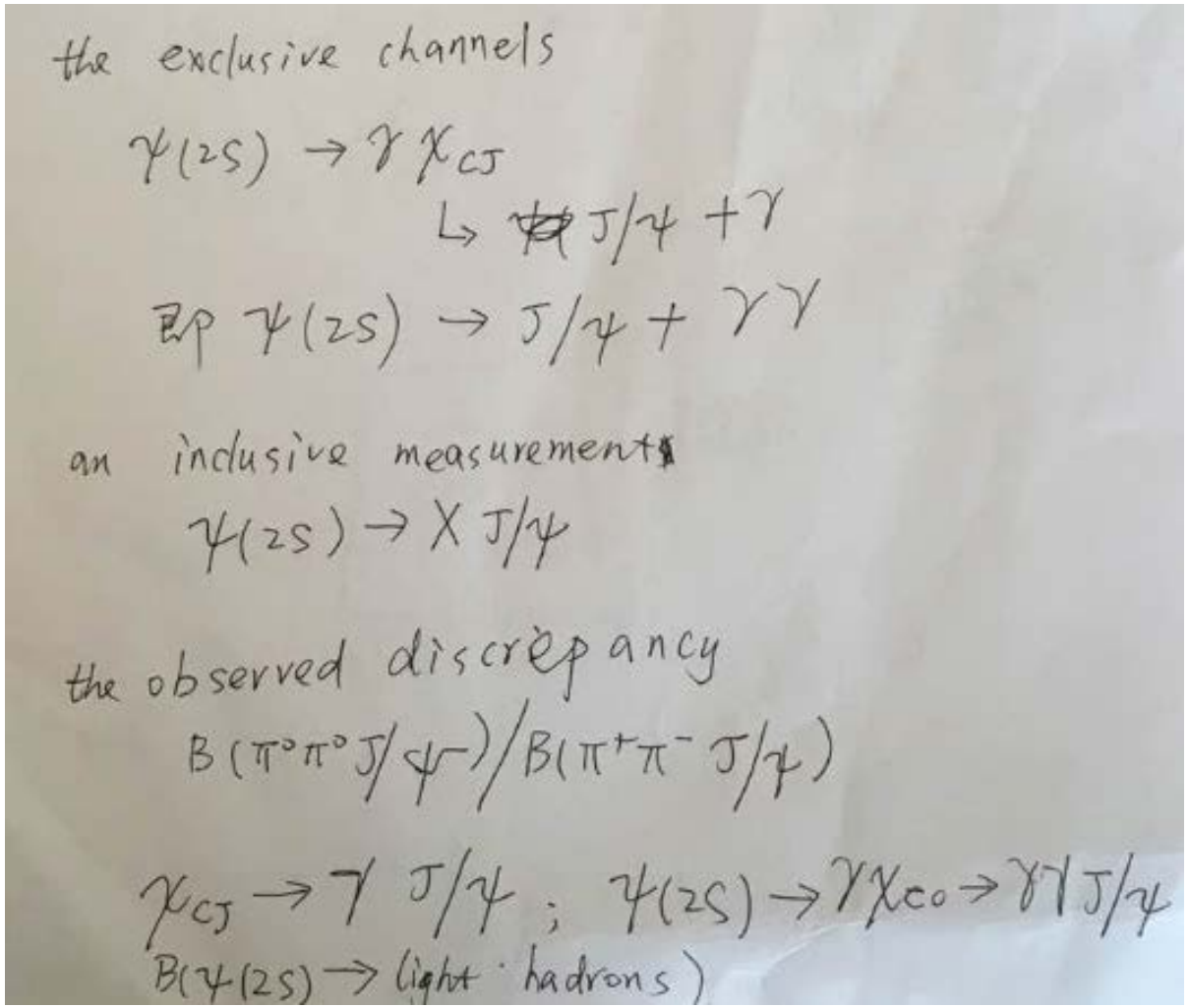
the exclusive channels
$\psi(2S) \to \gamma \chi_{cJ}$
$\hookrightarrow J/\psi + \gamma$
即 $\psi(2S) \to J/\psi + \gamma\gamma$
an inclusive measurement
$\psi(2S) \to X J/\psi$
the observed discrepancy
$B(\pi^0\pi^0 J/\psi) / B(\pi^+\pi^- J/\psi)$
$\chi_{cJ} \to \gamma J/\psi$; $\psi(2S) \to \gamma\chi_{c0} \to \gamma\gamma J/\psi$
$B(\psi(2S) \to$ light hadrons$)$

TABLE I. For each mode: the detection efficiency, ϵ, in percent; the numbers of events found in the $\psi(2S)$ and continuum samples, $N_{\psi(2S)}$ and $N_{\rm cont}$; the number of $\psi(2S)$ related background events, $N_{\rm bgd}$; the branching fraction in percent and its ratio to $\mathcal{B}_{XJ/\psi}$ and $\mathcal{B}_{\pi^+\pi^- J/\psi}$, also in percent.

Channel	ϵ	$N_{\psi(2S)}$	$N_{\rm cont}$	$N_{\rm bgd}$	$\mathcal{B}$	$\mathcal{B}/\mathcal{B}_{XJ/\psi}$	$\mathcal{B}/\mathcal{B}_{\pi^+\pi^- J/\psi}$
$\pi^+\pi^- J/\psi$	49.3	60344	221	113	$33.54 \pm 0.14 \pm 1.10$	$56.37 \pm 0.27 \pm 0.46$	
$\pi^0\pi^0 J/\psi$	22.2	13399	67	115	$16.52 \pm 0.14 \pm 0.58$	$27.76 \pm 0.25 \pm 0.43$	$49.24 \pm 0.47 \pm 0.86$
$\eta J/\psi$	22.6	2793	17	116	$3.25 \pm 0.06 \pm 0.11$	$5.46 \pm 0.10 \pm 0.07$	$9.68 \pm 0.19 \pm 0.13$
$\eta(\to \gamma\gamma)J/\psi$	16.9	2065	14	103	$3.21 \pm 0.07 \pm 0.11$	$5.39 \pm 0.12 \pm 0.06$	$9.56 \pm 0.21 \pm 0.14$
$\eta(\to \pi^+\pi^-\pi^0)J/\psi$	5.8	728	3	13	$3.39 \pm 0.13 \pm 0.13$	$5.70 \pm 0.21 \pm 0.13$	$10.10 \pm 0.38 \pm 0.22$
$\pi^0 J/\psi$	13.9	88	3	20	$0.13 \pm 0.01 \pm 0.01$	$0.22 \pm 0.02 \pm 0.01$	$0.39 \pm 0.04 \pm 0.01$
$\gamma\chi_{c0} \to \gamma\gamma J/\psi$	23.4	172	20	17	$0.18 \pm 0.01 \pm 0.02$	$0.31 \pm 0.02 \pm 0.03$	$0.55 \pm 0.04 \pm 0.06$
$\gamma\chi_{c1} \to \gamma\gamma J/\psi$	30.6	3688	46	21	$3.44 \pm 0.06 \pm 0.13$	$5.77 \pm 0.10 \pm 0.12$	$10.24 \pm 0.17 \pm 0.23$
$\gamma\chi_{c2} \to \gamma\gamma J/\psi$	28.6	1915	56	62	$1.85 \pm 0.04 \pm 0.07$	$3.11 \pm 0.07 \pm 0.07$	$5.52 \pm 0.13 \pm 0.13$
XJ/ψ	65.3	151 138	37916	123	$59.50 \pm 0.15 \pm 1.90$		

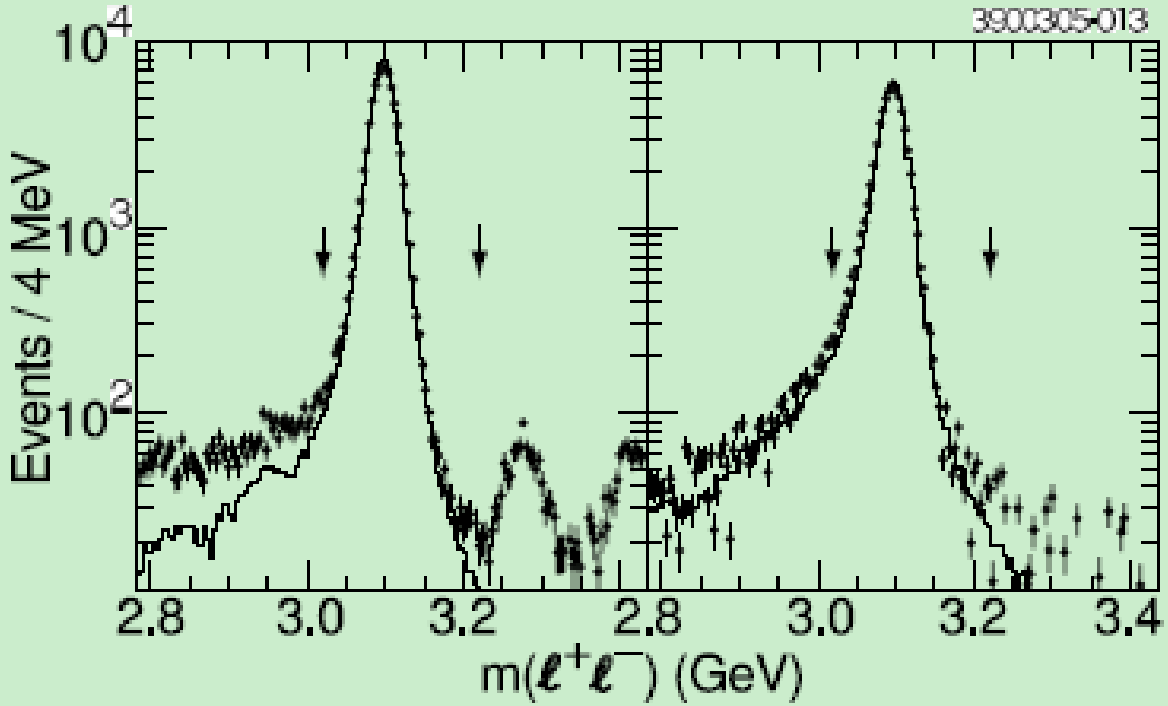

FIG. 1. For inclusively selected dimuon (left) and dielectron (right) events, the distributions of the dilepton mass in the $\psi(2S)$ data (solid circles), after subtraction of the luminosity-scaled continuum, and in MC (solid line). The two peaks above 3.2 GeV in the $m(\mu^+\mu^-)$ distributions correspond to backgrounds from $\chi_{c0,2} \to K^+K^-$ and $\chi_{c0} \to \pi^+\pi^-$.

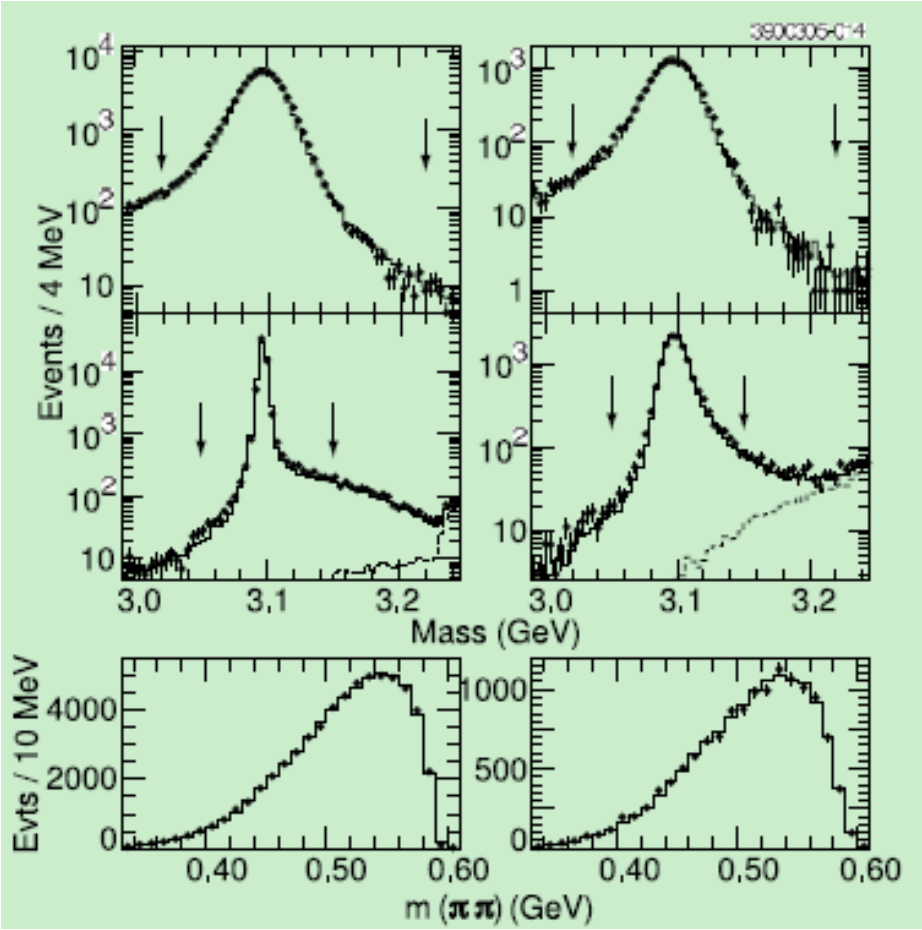

FIG. 2. For $\psi(2S) \to \pi^+\pi^-\ell^+\ell^-$ (left) and $\psi(2S) \to \pi^0\pi^0\ell^+\ell^-$ (right), e^+e^- and $\mu^+\mu^-$ samples combined, candidate events in the $\psi(2S)$ data (solid circles), MC simulation of signal (solid line), and $\psi(2S) \to \eta J/\psi$ background (dashed histogram): distributions of the dilepton mass (top), the mass recoiling against the dipion pair (middle), and the invariant mass of the two pions.

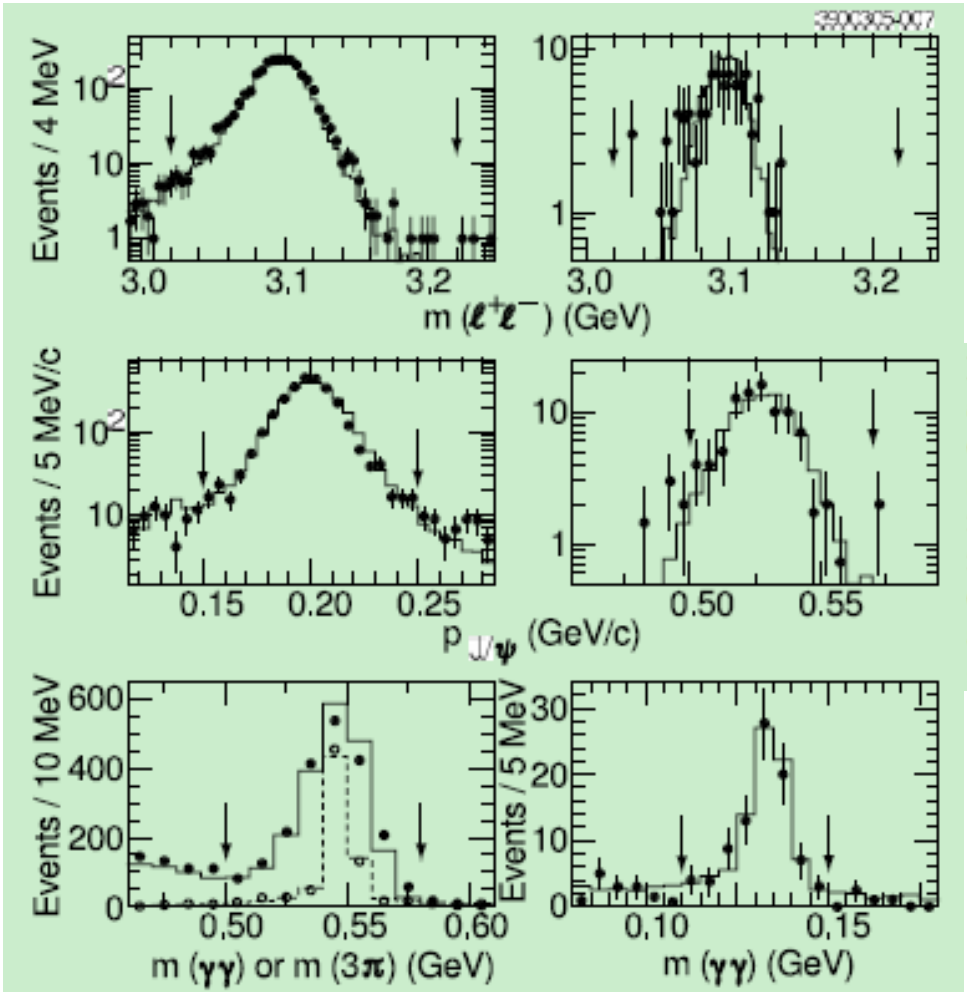

FIG. 3. For $\psi(2S) \to \eta(\to \gamma\gamma, \pi^+\pi^-\pi^0)\ell^+\ell^-$ (left) and $\psi(2S) \to \pi^0\ell^+\ell^-$ (right), e^+e^- and $\mu^+\mu^-$ samples combined, candidate events in the $\psi(2S)$ data (solid circles) and MC simulation of signal (solid line): distributions of the dilepton mass (top), the J/ψ momentum (middle), and the invariant mass of the two photons. In the lower left mass plot, the solid circles (data) and solid line (MC) apply to $\eta \to \gamma\gamma$ decays, and the open circles (data) and the dashed histogram (MC) to $\eta \to \pi^+\pi^-\pi^0$.

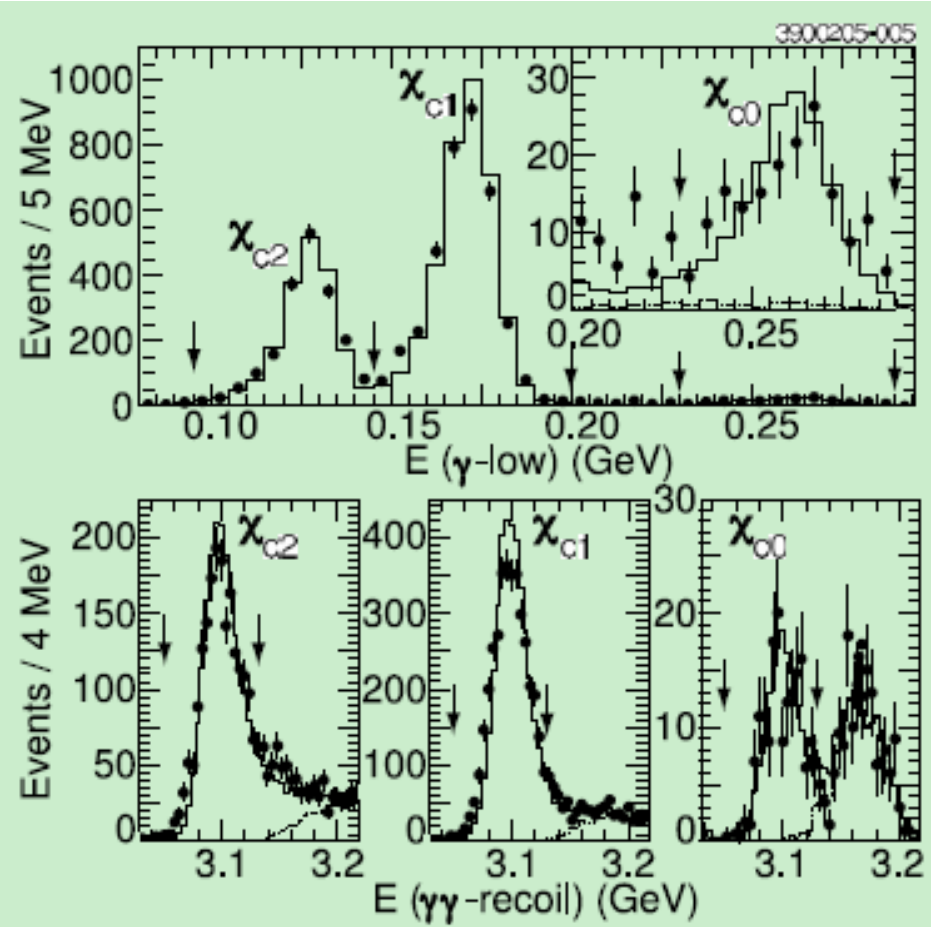

FIG. 4. For $\psi(2S) \to \gamma\chi_{cJ}$, $\chi_{cJ} \to \gamma J/\psi$, $J/\psi \to \ell^+\ell^-$ candidate events in the $\psi(2S)$ data (solid circles) and MC simulation of signal (solid line), the distribution of the energy of the second-most energetic photon, $E_{\gamma\text{-low}}$ (top), and the two-photon recoil mass (bottom). The arrows indicate nominal cut values. The inset offers a close-up of the χ_{c0} region. The broken lines represent $\pi^0\pi^0 J/\psi$ MC.

Summary

In summary, we have determined the branching fractions for all exclusive $\psi(2S) \to J/\psi + h$ ($h = \pi^+\pi^-, \pi^0\pi^0, \eta, \pi^0$) and $\psi(2S) \to \gamma\chi_{cJ} \to \gamma\gamma J/\psi$ transitions, with a similar strategy applied to all channels. We obtain results for $\mathcal{B}[\psi(2S) \to J/\psi + h]$ that are consistent with but more precise than previous measurements, where available, and $\mathcal{B}[\psi(2S) \to \gamma\chi_{cJ} \to \gamma\gamma J/\psi]$ values both larger and more precise than previous measurements. The analysis is complemented by a study of the inclusive mode $\psi(2S) \to XJ/\psi$, the production rate of which is seen to be consistent with that of the sum of all expected exclusive contributions. Ratios between the branching fractions as well as results on $\mathcal{B}(\chi_{cJ} \to \gamma J/\psi)$ are also tendered.